Chemical Engineering Journal 165 (2010) 658–667

Contents lists available at ScienceDirect

Chemical Engineering Journal

journal homepage: www.elsevier.com/locate/cej

A study on the oxidation of phenol by heterogeneous iron silica catalyst

Farook Adam*, Jeyashelly Andas, Ismail Ab. Rahman

School of Chemical Sciences, Universiti Sains Malaysia, 11800 Penang, Malaysia

ARTICLE INFO

Article history:
Received 19 June 2010
Received in revised form 1 September 2010
Accepted 10 September 2010

Keywords:
Iron catalyst
Silica
Rice husk
Oxidation of phenol
Catechol

ABSTRACT

A series of iron silica catalyst with (5–20) wt.% Fe^{3+} were prepared by means of a simple solvent extraction and sol–gel technique. These catalysts were probed for the oxidation of phenol employing hydrogen peroxide. Catalytic performance increased up to 10 wt.% Fe^{3+} loading. Further increase in the iron content was found to reduce the phenol conversion rate. Higher Fe^{3+} loading (>10% Fe^{3+}) resulted in smaller pore size and exhibited extra framework Fe^{3+} in the catalyst, which lead to catalytic deficiency in phenol oxidation. Phenol oxidation by RH-10Fe gave 95.2% conversion at 343 K with selective formation of 61.3% catechol (CAT) and 38.7% hydroquinone (HQ). Reusability studies with RH-10Fe resulted in only 16% loss in catalytic activity. However, no leaching of iron was detected. The CAT/HQ ratio was found to be constant during the reaction which suggested a non-free radical catalytic mechanism to be operative.

1. Introduction

Phenol is a foremost pollutant in UESEPA list with limits of discharge less than 0.5 mg L^{-1} [1]. This is a lethal and hazardous contaminant which is believed to be carcinogenic. Many investigators are currently engaged in finding ways to eliminate this pollutant from the environment. Specific chemical processes are necessary to convert this carcinogenic compound into industrially benign products such as diphenols. Diphenols, namely catechol (CAT) and hydroquinone (HQ) are used for diverse applications such as photographic chemicals [2], polymerization inhibitors, antioxidants and flavoring agents [3,4]. In the oxidation of phenol, hydrogen peroxide appears to be an appropriate and potential oxidant due to high oxygen content and yielding water as the only by-product [5,6]. Hydrogen peroxide is known to be less of an environmental pollutant [7,8]. Many attempts to oxidize phenol by aqueous hydrogen peroxide had been reported [9–12] with a variety of heterogeneous catalysts.

The invention of titanium silicate, TS-1, by Enichem has indeed opened a remarkable application of heterogeneous catalyst in the oxidation of phenol. However, some characteristics exhibited by TS-1, such as complex preparation method and small pore size restrict its use in the oxidation of large molecules. It also has an inherent difficulty during separation due to its small size particles which has limited its function in the oxidation of phenol [13]. This has stimulated much research to develop cheaper and better catalysts which are capable of converting this toxic compound into more benign and useful products.

Rice husk (RH), which is a by-product from the rice processing industry, is found abundantly in most rice producing countries. Burning seems to be an easy way of disposing the husks. However, this can lead to environmental problems [14]. Biodegradation of the RH is also a slow process due to the high silica content. Therefore, utilization of RH as an alternative source of silica had gained some interest.

Recently, silica from RH had been used as catalyst support for important industrial applications such as oxidation of cyclohexane [15,16], cyclohexene and cyclohexanol [16], oxidation of phenylmethanol [17] and decomposition of cyclohexanol [18]. The high catalytic behavior of these silica supported catalysts is due to the high surface area of the resulting catalysts. Several publications have appeared on iron supported rice husk ash silica. Adam et al. [19] had reported the catalytic activity of iron incorporated rice husk ash silica for benzylation of toluene. The synthesis of iron supported rice husk ash silica as a catalyst for the benzylation of xylene had also been reported [20]. However, in both of these cases, the rice husk was pyrolyzed into ash which required high consumption of energy. To overcome this, Adam and Andas [21] found a cheaper way to extract the silica by solvent extraction and incorporated the metal via a sol–gel technique at room temperature. In this present studies, we extend the use of the iron loaded rice husk silica catalyst in the oxidation of pollutants such as phenol.

Various sources of silica have been used as catalyst support for the oxidation of phenol [22–25]. However, there is no published literature of silica from rice husk being used as catalyst support for the oxidation of phenol. While there is no real advantage on using silica from RH, however, it certainly creates added value to the otherwise useless waste material. An added advantage of this procedure will also result in the husk becoming more amenable to biological degradation and ease the disposal problem for RH.

* Corresponding author. Tel.: +60 4 6533567; fax: +60 4 6574854.
E-mail addresses: farook@usm.my, farook_dr@yahoo.com (F. Adam).

1385-8947/$ – see front matter © 2010 Elsevier B.V. All rights reserved.
doi:10.1016/j.cej.2010.09.054

In the relentless search for an environmentally friendly and active heterogeneous catalyst, we have synthesized a high surface area iron incorporated silica catalyst for the oxidation of phenol from RH. This work discusses the preparation of an environmental friendly catalyst from rice husk, its characterization and its catalytic activity in the oxidation of phenol.

2. Experimental

2.1. Materials

Analytical reagent grade ferric nitrate, $Fe(NO_3)_3{\cdot}9H_2O$ (98.5%) was obtained from Bendosen. Acetophenone and analytical grade phenol (Sigma–Aldrich, 99.0%) were checked by GC and used without further purification. Hydrogen peroxide (30 wt.%) was procured from J.T. Baker and used as obtained. All other chemicals were of analytical grade.

2.2. Catalyst preparation and characterization

The method used for the pretreatment and extraction of sodium silicate from RH were similar to that reported previously [17]. In a typical extraction, 30 g of dried RH was added into 500 mL of 1.0 M nitric acid and magnetically stirred for 24 h. The RH was made free from NO_3^- by washing thoroughly with distilled water. The acid treated RH was dried overnight in an oven at 383 K and its respective mass (denoted as RH-HNO_3) was recorded. The dried RH was then vigorously stirred in 500 mL of 1 M NaOH for 24 h to yield sodium silicate (dark brown) solution which was suction filtered and kept for further use. The residue was collected and dried in an oven at 383 K for 24 h. The mass of this residue was recorded (denoted as RH-NaOH). The mass difference between RH-HNO_3 and RH-NaOH was attributed to the mass of silica extracted from rice husk, i.e. 6.44 g.

The sodium silicate solution obtained was titrated slowly ($1.0\,mL\,min^{-1}$) with 3.0 M HNO_3 or 3.0 M HNO_3 containing the appropriate mass of $Fe(NO_3)_3{\cdot}9H_2O$ to get 5, 10, 15 and 20 (wt.%) of Fe^{3+} until pH 3.0 was reached. The resulting gel solution was aged in the mother liquor for 2 days at room temperature. The gel was recovered by centrifugation at 4000 rpm (Hettich Zentrifugen, model Rotina 38), washed thoroughly with distilled water and dried in an oven at 383 K for 18 h. The product was ground and denoted as RH-Si while the iron loaded samples were designated as RH-*x*Fe (*x* = 5, 10, 15 and 20, denoting wt.% of Fe^{3+} used).

BET specific surface area, BJH adsorption and desorption, pore volume and pore size distribution were measured by N_2 adsorption (Micromeritics Instrument Corporation model ASAP 2000, Norcross) porosimeter. FT-IR spectra were recorded on a Perkin Elmer System 2000 with wave number ranging from 4000 to 400 cm^{-1} using pressed KBr pellets. Phase identification of the samples were performed on Kristallofex Siemens, model D5000 X-ray diffraction instrument equipped with Cu K_α radiation ($\lambda = 1.50$ Å). The iron content of the catalysts were determined by atomic absorption spectroscopy (AAS, Perkin Elmer 3100) after an appropriate sample preparation described as below. Diffuse reflectance UV–vis spectra of the catalysts were collected on a Lambda 35 UV–visible spectrometer (Perkin Elmer) in the 200–600 nm wavelength range employing KBr as blank. The solid state ^{29}Si MAS NMR spectra were obtained on a Bruker DSX-3000 with relaxation time of 20 s, pulse width of 5 s and relaxation delay of 20 s. Chemical shifts were referenced to tetramethylsilane (TMS).

To analyze for iron, a catalyst sample of mass 50 mg was digested in 0.5 mL aqua regia (HNO_3:HCl ≡ 1:3, v/v) and 3 mL HF in a Teflon container. The sample was heated at 383 K for 1 h and cooled to RT. Into this sample, 0.5 g of H_3BO_3 in 10 mL double de-ionized water was added and the sample was made up to 100.0 mL with double de-ionized water. This sample was analyzed using atomic absorption spectroscopy.

2.3. Oxidation of phenol by H_2O_2 using RH-xFe (x = 5, 10, 15 and 20)

The oxidation of phenol was carried out in a 50 mL double necked round bottom flask fitted with a water-cooled condenser. In a typical run, phenol (1.88 g, 20 mmol) was dissolved in 10 mL of water. The mixture was transferred into a round bottom flask containing 30 mg of activated RH-10Fe as catalyst which was immersed in a temperature controlled oil bath at 343 K. Once the reaction temperature was stabilized, H_2O_2 (2.28 g, 20 mmol) was added drop wise to the vigorously stirred (600 rpm) reaction mixture. Aliquots of the reaction mixture ($0.5\,cm^{-3}$) were periodically withdrawn using a syringe. This was mixed with 20 μL of acetophenone as an internal standard and analyzed by GC (Clarus 500, Perkin Elmer) equipped with flame ionization detector and fitted with a capillary column – Elite-Wax, 30 m × 0.32 mm i.d. The identities of the respective products were confirmed by GC–MS (Clarus 600, Perkin Elmer). The products were further confirmed by comparing the GC of the respective pure catechol and hydroquinone. Phenol conversion and selectivity of the products were calculated respective to the area of the internal standard used. All reactions were performed in triplicate and average values are used in data presentation.

The concentration of residual H_2O_2 was determined by an iodometric titration with sodium thiosulphate (0.1 N) in the presence of starch as an indicator [26]. Aliquot of samples were withdrawn during the reaction and was quickly subjected to the titration.

2.3.1. Leaching and reusability of the catalysts

Leaching of ferric ions from the catalyst was determined by filtering off the catalyst from the reaction mixture after 2 min by using hot filtration technique. The reaction mixture before filtration was analyzed by GC as before. The hot filtrate was transferred without delay into a round bottom flask which had been immersed in oil bath at the same temperature. The reaction was allowed to continue for an additional 2 h (without the catalyst) and the course of the reaction was monitored periodically by GC. For further confirmation, a blank reaction was carried out at 343 K in the presence of 30 mg RH-10Fe, 4.53 g H_2O_2 and 10 mL of water as reported by Maurya et al. [27].

The reusability was studied by regenerating the catalyst by washing with copious amount of distilled water, followed by acetone and dried in an oven at 383 K for 24 h. The catalyst was collected and reused for further runs as described earlier.

3. Results and discussion

3.1. Characterization of the catalysts

3.1.1. Nitrogen adsorption–desorption isotherms and elemental analysis

Incorporation of different iron content did not affected the N_2 sorption isotherm and it's desorption hysteresis loop (Fig. 1). RH-Silica showed H2 hysteresis loop which are usually observed for ink bottle shaped mesopores [28] while all the iron loaded catalysts showed H1 hysteresis. H1 is observed for compacts of spheroidal particles of uniform size and arrays [21]. This is in agreement with uniform pore size distribution (PSD) of RH-5Fe and RH-10Fe. All five catalysts showed isotherm of Type IV according to IUPAC classification. Type IV isotherm is normally observed for mesoporous solids [29,30]. However, RH-20Fe exhibits a sigmoid type isotherm with a closure of the loop at relative pressure very close to 0. This type

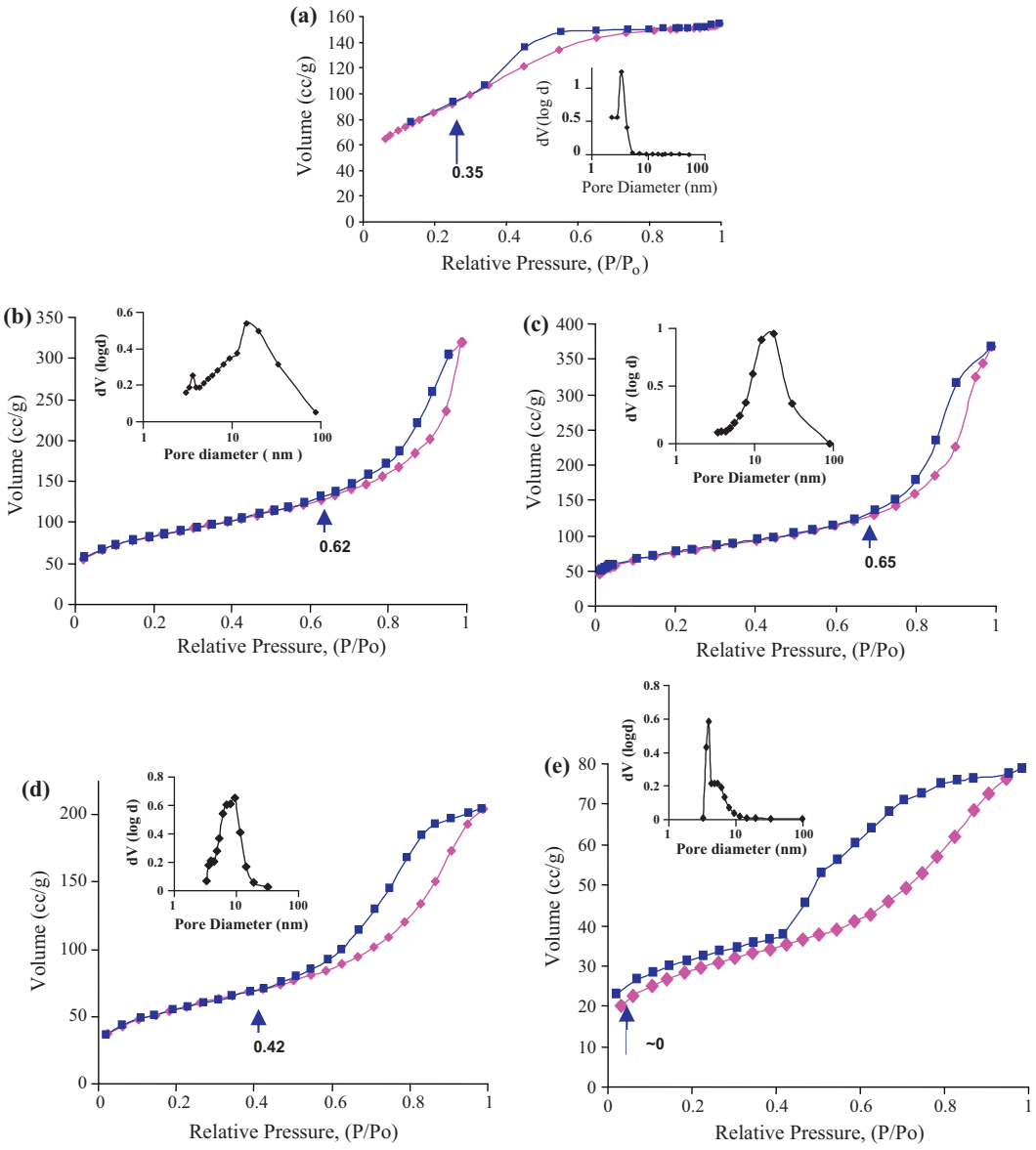

Fig. 1. The N_2 adsorption desorption isotherms of (a) RH-Silica, (b) RH-5Fe, (c) RH-10Fe, (d) RH-15Fe and (e) RH-20Fe. Insets are the respective pore distribution plots. → Hysteresis inflection point.

of isotherm is normally obtained for adsorbent which has swelling tendencies [15].

The capping of pores by increasing amount of metal resulted in RH-20Fe having a narrow PSD. The excess metal ions had also resulted in RH-20Fe exhibiting swelling characteristics. This could result from the accumulation of metal species between the silica lattices resulting in an open pore structure. This leads to large voids which enable the swelling tendencies.

An increase in volume of N_2 adsorbed from RH-5Fe to RH-10Fe indicates the increasing number of pores in the respective samples. However, the decrease in volume of N_2 adsorbed for RH-15Fe and RH-20Fe reflects the decreased number of pores.

Table 1 summarizes the textural properties and the iron content calculated from AAS analysis. It can be seen that the incorporation of iron leads to a decrease in the BET surface area as the loading of Fe^{3+} increased from 5 to 20 wt.%. A similar trend was also observed by Baiker and co-workers [31] in the synthesis of iron-oxide silica aerogels. The reduction in specific surface area of ca. 65% was probably due to the capping of the pores by the loaded metal [32,33]. This observation was inline with the resulting decrease in pore volume. Elemental analysis by AAS clearly showed that the actual metal loading was less than the iron used during the preparation.

3.1.2. X-ray diffraction and FTIR analysis

X-ray diffraction pattern (not shown) of RH-Silica and the iron loaded catalysts were found to be amorphous [34,35]. A gradual decrease in intensity of the broad peak was observed as the iron loading increased from 5 to 20 wt.%. This indicates possible structural changes from amorphous to crystalline, which however could not be detected due to the microcrystalline nature of the particles. Generally, iron is a cubic element with a plane of symmetry which can be identified by XRD due to its opaque characteristics towards light. However, in this study, iron loaded catalysts were found to be amorphous which could be due to the well dispersed nature of the iron particles on the amorphous silica support. This should result in a good dispersion of the Fe^{3+} within the silica matrix – thus preventing the aggregation of the iron atoms to form the crystalline phase.

Fig. 2 shows the FT-IR spectra of the catalysts. Most of the FTIR bands of silica from RH and metal loaded silica from RH had been

Table 1
Textural properties and iron chemical analysis data of the prepared catalysts.

Catalyst	SBET ($m^2\ g^{-1}$)	Average pore volume ($cc\ g^{-1}$)	Average pore diameter (nm)	Iron loading (%)
RH-Silica	312	0.27	3.0	–
RH-5Fe	282	0.42	10.0	4.88
RH-10Fe	259	0.51	12.0	7.85[a](7.38)[b](6.58)
RH-15Fe	190	0.28	6.0	14.20
RH-20Fe	96	0.11	4.0	15.47

[a] Iron content after leaching test (fresh used).
[b] Iron content after 4th reused analysis.

well characterized [14–17,20,21,36,37]. However, two of the main features to note from Fig. 2 are (a) the Si–O–Si bond ($1090\ cm^{-1}$) was found to show a red shift as the iron content was increased from 5 ($1082\ cm^{-1}$) to 20 wt.% ($\sim 1065\ cm^{-1}$), and (b) upon increase in iron loading, the peak intensity at $972\ cm^{-1}$ which was assigned as Si–OH bond was found to decrease. The decrease in intensity of the $972\ cm^{-1}$ band showed the progressive formation of the Si–O–Fe bond structure [22]. This together with the red shift in the $1090\ cm^{-1}$ band is a good indication that the Si–O–Fe bond structure had formed.

3.1.3. The diffuse reflectance UV–vis spectrum

As illustrated in the DR UV–vis spectra (Fig. 3), a strong absorption band in the region 245–250 nm can be attributed to the dπ–pπ charge transfer transition between iron and oxygen (ligand) atoms [38,39]. These respective bands are suggested to be due to four coordinated Fe^{3+} in tetrahedral positions which appear due to $t_1 \rightarrow t_2$ and $t_1 \rightarrow e$ transitions [40,41]. The band at ca. 320 nm was correlated to the Fe–O charge transfer transitions obtained for RH-10Fe [42]. Spectra of both RH-15Fe and RH-20Fe show the presence of extra framework Fe^{3+} ions at ca. 350, 400 and 500 nm. The band which appears as a shoulder at ca. 350 nm corresponds to oligomerized iron species and Fe^{3+} agglomeration [43]. The absorption bands above 400 nm indicate the presence of large particles of iron oxide [44]. The band around 500 nm arises due to Fe^{3+} in aggregate forms [45,46]. However, a very broad band results for RH-15Fe and RH-20Fe in this region. This shows that aggregates of Fe^{3+} species are most likely absent or in very low concentration. The 400 and 500 nm bands were surprisingly absent in RH-5Fe and RH-10Fe. This clearly shows a transformation of iron state from isolated species to bulk aggregate structure as iron loading increased from 5 to 20 wt.%.

It should be noted that the DR UV–vis spectrum is quite different for RH-15Fe and RH-20Fe. This is certainly due to the different structural morphology of the catalysts with increasing metal content.

3.1.4. ^{29}Si MAS NMR analysis

The ^{29}Si MAS NMR spectra of RH-Silica and Fe/Silica catalysts with different iron content are shown in Fig. 4. The spectrum of the parent RH-Silica exhibits two shifts with mean values of −101.4 and −110.7 ppm. These peaks are assigned as Q^3 (3Si, 1OH) and Q^4 (4Si) units respectively [47]. Sample with 5 wt.% Fe^{3+} show only one intense peak at −109.6 (Q^4). The plausible reason for the non-existence of Q^3 signal in RH-5Fe may be due to the low degree of substitution and also due to the overlap with its intense Q^4 signal. For RH-10Fe, it exhibits the presence of a shoulder peak at −100.4 (Q^3) and −108.7 ppm (Q^4). Further increase in the iron loading to 15 and 20 wt.% Fe^{3+}, leads to the disappearance of Q^4 signal. Hence, the presence of Q^3 signals for RH-10Fe (−100.4), RH-15Fe (−102.3) and RH-20Fe (−105.8) indicates the presence of Si–(O–Fe) linkage [48] in which silica is tetrahedrally coordinated via oxygen to one Fe and three silicon atoms [49,50]. Excluding RH-Silica, all the iron loaded silica catalysts show the presence of spinning side bands which suggests the paramagnetic nature of Fe(III) species [50]. This observation confirms the successful incorporation of Fe into the silica framework and similar result has been reported by Testa et al. [51]. The Q^4 intensity of RH-Silica is higher than that of other Fe/silica catalysts. Zhao et al. [52] have reported similar observation for Fe-MCM-48 catalyst. This is presumably due to the steric restraint resulting from introducing guest atoms such as Fe with different size into the silicon framework and also due to minimum intertetrahedral bond angles of Si–O–Si and Si–O–Fe linkage [53]. Increasing the amount of Fe lead to difficulty in condensation of silanol groups and finally reduced the framework connectivity [48,52,53] as observed for higher iron loaded catalysts (RH-15Fe and RH-20Fe).

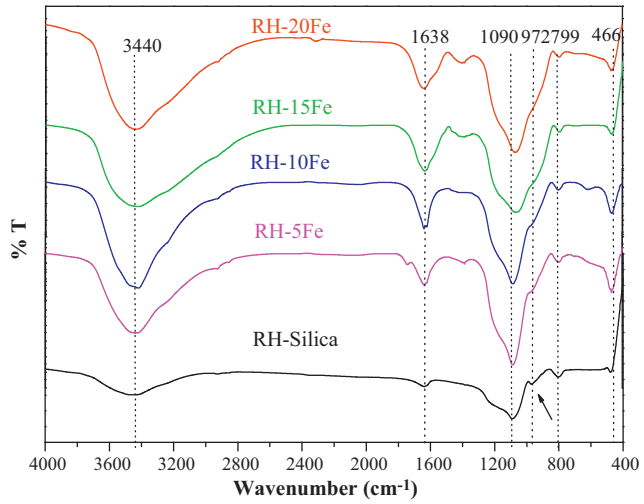

Fig. 2. The FT-IR spectra of catalysts.

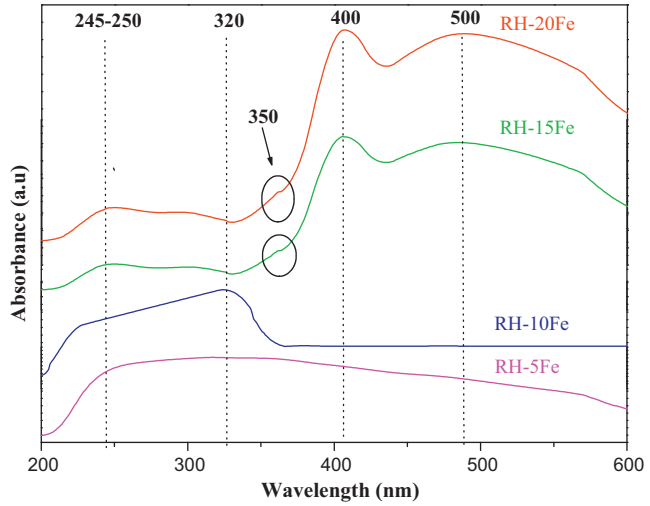

Fig. 3. The DR UV–vis spectra of catalysts.

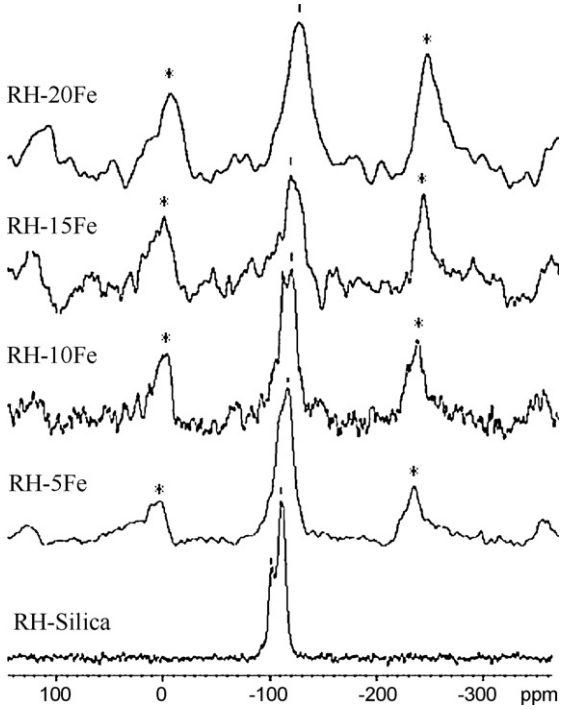

Fig. 4. [29] Si MAS NMR spectra of catalysts (the asterisks indicate spinning side bands).

3.2. Catalytic activity – the oxidation of phenol

All the iron loaded catalysts together with RH-Silica were evaluated for the oxidation of phenol. Oxidation of phenol was found to yield catechol (CAT) and hydroquinone (HQ) as the only products. In order to optimize the reaction conditions, RH-10Fe was used to investigate the effect of reaction temperature, catalyst mass, molar ratio of reactants, the effect of solvent type and metal loading. Leaching and reusability of the catalyst was also determined.

3.2.1. The effect of reaction temperature

Generally, the reaction temperature has a considerable effect on the oxidation of phenol. Thus, in this study, catalytic activity was tested over different temperatures, ranging from 303 (room temperature) to 353 K and the results are shown in Fig. 5. An increase in temperature up to 343 K resulted in enhanced phenol conversion from 43.3% at 303 K to 68.0% at 343 K. However, further increase in the reaction temperature to 353 K did not show any significant enhancement in phenol conversion (68.3%). Nevertheless, a progressive decrease in CAT selectivity was observed as the reaction temperature was increased. A plausible reason for the decrease in catalytic activity at 353 K was the thermal decomposition of H_2O_2 which is greatly enhanced at elevated temperatures. Similar observation had been reported for other iron containing catalysts [22,54]. Based on the results obtained, 343 K was determined as the optimal reaction temperature for phenol oxidation with RH-10Fe. It is noteworthy that even at room temperature (303 K), RH-10Fe afforded phenol conversion of ca. 43%. Suja and Sugunan [55] reported 81.5% conversion at 30 °C using 100 mg of iron promoted sulfated zirconia and H_2O_2:phenol ratio of 5:1. This shows the highly active nature of the RH-10Fe for the oxidation process compared to these reported catalysts. It also indicates that a free radical mechanism may not be operating in this catalytic system.

3.2.2. The effect of catalyst mass

The catalyst mass was varied from 10 to 70 mg (Fig. 6). As the mass of the catalyst increased, the conversion increased from 62.7 to 66.4 (%) for 10 and 20 mg of catalyst. The maximum phenol conversion of 68.0% was obtained when 30 mg of catalyst was used. Further increase in the catalyst mass to 70 mg, resulted in a progressive decrease in the conversion to 61.6%. The rationale for this could be the larger amount of catalyst presents a very much higher surface area for the H_2O_2 to dissociate, i.e. too fast to form the active intermediate to affect oxidation. However, these variations in the conversion seem to be at best, marginal and may not be significant.

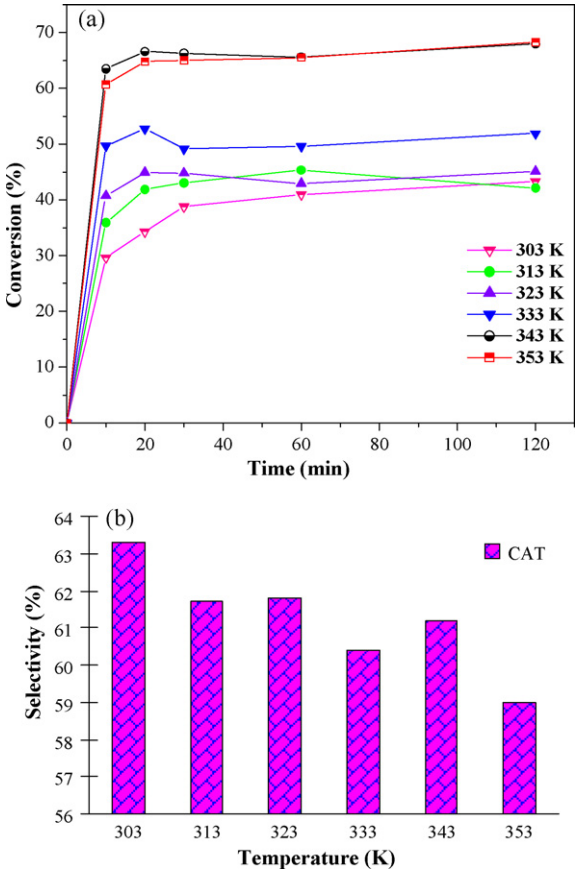

Fig. 5. The reaction profiles at different temperatures. (a) The percentage conversion with respect to time at different reaction temperature and (b) the variation in the selectivity of catechol with respect to temperature. Reaction conditions: phenol:H_2O_2 (molar ratio) 1:1; catalyst used = RH-10Fe; mass of catalyst = 30 mg; solvent = water (10 mL); reaction time = 2 h.

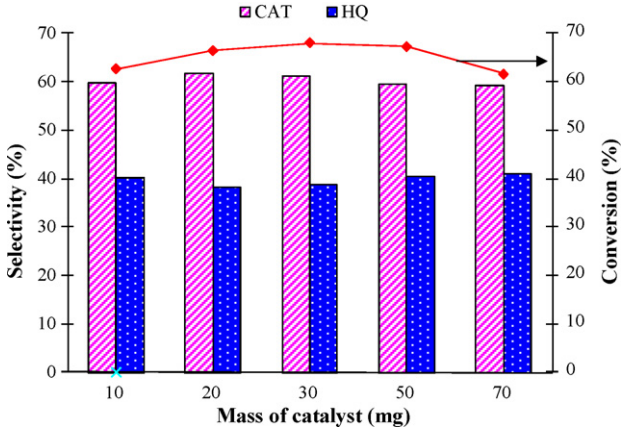

Fig. 6. A graph of percentage selectivity and conversion with respect to the mass of catalyst used. Reaction conditions: phenol:H_2O_2 (molar ratio) 1:1; catalyst = RH-10Fe; T = 343 K; solvent = water (10 mL); reaction time = 2 h.

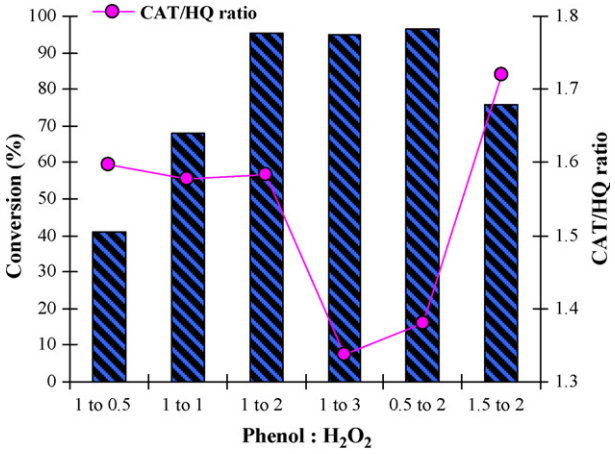

Fig. 7. Bar graph showing the effect of H_2O_2 concentration on phenol conversion and CAT/HQ ratio. Reaction conditions: catalyst used = RH-10Fe; mass of catalyst = 30 mg; T = 343 K; solvent = water (10 mL); reaction time = 2 h.

The product selectivity was found to remain consistently at 60.0% CAT and 40.0% HQ throughout the mass variation study. Nonetheless, from this study it can be concluded that 30 mg of catalyst gave the maximum conversion of phenol.

3.2.3. The effect of molar ratio of reactants

The molar ratio of phenol to H_2O_2 was investigated and the results are presented in Fig. 7. The conversion of phenol was found to increase drastically with an increase in H_2O_2 amount. At the lower molar ratio (1:0.5), phenol conversion was found to be 41.0% and showed a progressive increase to 95.2% at a molar ratio of 1:2. However, further increase in the H_2O_2 molar ratio to 1:3 did not show significant improvement in phenol oxidation. Nevertheless, the formation of HQ increased when the molar ratio was 1:3 (i.e. CAT/HQ decrease). The impact of H_2O_2 molar ratio towards product distribution was reflected in the decrease of CAT/HQ ratio at 1:3 molar ratios (Fig. 7). Surprisingly, increasing the molar ratio from 1:0.5 to 1:2, there was no major change in the CAT selectivity, i.e. it remained at ca. 61.2%. Based on these results, the optimum molar ratio was fixed at 1:2 due to the higher phenol conversion and moderate CAT selectivity.

By fixing the molar concentration of H_2O_2 and varying the phenol in molar ratio of 0.5:2 and 1.5:2, results in an increase in CAT selectivity ((CAT/HQ) increased). At a molar ratio of 0.5:2, the conversion reached maximum activity yielding 96.4% but with a higher selectivity for HQ. This suggests that by varying the molar ratio of the reactants, the required product can be selectively synthesized. This will be advantageous as HQ is the more sort after product in the industry. The lower conversion at molar ratio of phenol:H_2O_2 of 1:0.5 may be due to insufficient amount of H_2O_2 to react with the large excess of phenol. With the increasing phenol:H_2O_2 molar ratio from 0.5:2 to 1:2 and 1.5:2, it leads to selective CAT formation in which CAT/HQ ratio increase from 1.38 to 1.58 and 1.72 respectively. This clearly indicates that only at lower phenol concentration, formation of HQ becomes more favorable. However, as to why this *para*-dihydroxybenzene isomer is more favorable at lower phenol concentration is not well understood at this point. Based on the results obtained, a moderate ratio of phenol to H_2O_2 of 1:2 was chosen as the optimum condition.

3.2.4. The effect of solvent

Many studies had reported the influence of different solvents on phenol oxidation rate and its product distribution [56,57]. Hence, several solvent systems such as water, acetonitrile, methanol and dioxane were investigated. It was observed that phenol conversion was much higher when water was used as the solvent compared to others (Table 2). The conversion showed the following trend with respect to the solvent used: water (95.2%) > acetonitrile (59.3%) > methanol (37.9%) ≫ dioxane (0%). No reaction was observed in dioxane. It had been reported that there are three attributes which influence the selection of a solvent. These are (a) donor potential (DN), (b) acceptance ability (AN) and (c) polarity of the respective solvent [57]. Thus, as shown in Table 2, the DN/AN ratio decreases from 0.73 to 0.48 and 0.33 for acetonitrile, methanol and water respectively. The DN/AN ratio support the higher conversion observed in acetonitrile compared to methanol. However, explanation in terms of DN/AN ratio could not be applied for water. Thus, the contradictory performance of RH-10Fe in water medium was probably due to its high polarity. However, surprisingly, CAT formation was facilitated more in the solvent order methanol > acetonitrile > water. Considering the environmental factors and higher phenol conversion, water was selected as the best solvent for the oxidation of phenol.

Table 2
Variation in phenol conversion, product distribution and CAT/HQ ratio under different solvents studied.

Solvent	DN/AN[a]	Conversion (%)	Product distribution (%)		
			CAT	HQ	CAT/HQ
H_2O	0.33	95.2	61.3	38.7	1.58
$CH_3C{\equiv}N$	0.73	59.3	63.6	36.4	1.75
CH_3–OH	0.48	37.9	69.6	30.4	2.30
Dioxane	–	–	–	–	–

Reaction conditions: phenol:H_2O_2 (molar ratio) 1:2; catalyst = RH-10Fe; mass of catalyst = 30 mg; T = 343 K; solvent = (10 mL); reaction time = 2 h.
[a] Mal and Ramaswamy [57].

3.2.5. The effect of metal loading

To study the potential of iron loaded catalysts, experiments under optimized reaction conditions were carried out for RH-Silica (control), ferric nitrate (metal salt – as a homogeneous catalyst) and without any catalyst. These results are shown in Table 3. RH-Silica was found to be inactive in the oxidation of phenol. No measurable activity was recorded in the presence of only phenol and 30% H_2O_2, which shows that the catalyst was necessary for the reaction to occur. In order to clarify any contribution of dissolved Fe^{3+} from the precursor, the salt $Fe(NO_3)_3{\cdot}9H_2O$, was used as a homogeneous catalyst in the oxidation of phenol under similar reaction condition. It was noted that the use of this metal salt resulted in only 56.5% phenol conversion. Its selectivity was similar to RH-10Fe, i.e. 65.3% CAT and 37.9% HQ. Iron content in the catalyst was found to play a key role in controlling the performance of iron silica catalysts in phenol oxidation. This hypothesis was supported by the data presented in Table 3. Phenol conversion obtained for RH-5Fe, RH-10Fe, RH-15Fe and RH-20Fe were found to be 85.8, 95.2, 88.6 and 85.0% respectively. A significant increase in the conversion was evident up to

Table 3
Comparative reaction profile of catalysts in the oxidation of phenol by H_2O_2.

Catalysts	Conversion (%)	*Productdistribution*(%)	
		CAT	HQ
No catalyst	0.0	–	–
RH-Silica	0.0	–	–
$Fe(NO_3)_3.9H_2O$	56.5	65.3	34.7
RH-5Fe	85.8	57.6	42.4
RH-10Fe	95.2	61.3	38.7
RH-15Fe	88.6	56.6	43.4
RH-20Fe	85.0	55.7	44.3

Reaction conditions: phenol:H_2O_2 (molar ratio) 1:2; catalyst = 30 mg; T = 343 K; solvent = water (10 mL); reaction time = 2 h.

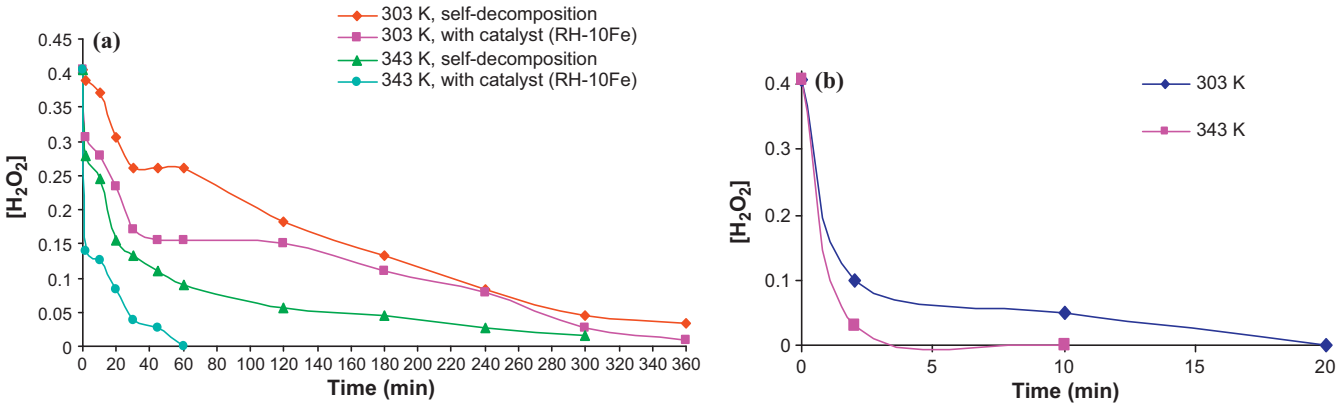

Fig. 8. The residual concentration of H_2O_2 over reaction time in 10 mL water in the presence of (a) 4.53 g H_2O_2 only at 303 and 343 K and (b) phenol = 1.88 g, H_2O_2 = 4.53 g and 30 mg RH-10Fe at 303 and 343 K.

10 wt.% Fe^{3+} loading. However, further increase in the iron loading lead to a decrease in the catalytic activity. This was also accompanied with a fall in selectivity of CAT and CAT/HQ ratio. These results clearly showed that upon increasing iron loading >10 wt.%, formation of HQ was facilitated. In explaining the higher performance of RH-10Fe, these findings can be inferred to the presence of wider pores in RH-10Fe, i.e. 12 nm, and higher surface area (N_2-sorption analysis).

It is suggested that larger pore diameter would easily allow the reactants (phenol and H_2O_2) to approach the inner active sites of the catalyst. Hence, for RH-10Fe, high pore diameter and well-dispersed iron species in the silica matrix allowed accessibility of the reactants to the active sites for the reaction to take place. Besides this, high pore volume of RH-10Fe compared to other iron loaded catalysts enabled the accommodation of more active phases for the reaction to occur. Contrast to this phenomenon, results showed that there was no improvement in the catalytic activity as the iron loading increased from 15 to 20 wt.% Fe^{3+}. This correlated well with the low surface area of RH-15Fe and RH-20Fe as shown in Table 1. For RH-15Fe and RH-20Fe, characteristic features of low surface area and pore volume reduced the catalytic activity compared to RH-10Fe. High iron concentration can actually cause blocking of the pores which can cut off some of Fe^{3+} active sites deep within the catalyst matrix. This can effectively reduce the specific surface area of the catalysts resulting in the lowering of catalytic activity [58].

On the other hand, the narrower pore diameter of RH-20Fe could restrict the bulky molecules such as phenol to approach the active sites. Additionally, appearance of extra iron species as shown in DR UV–vis spectra for RH-15Fe and RH-20Fe was found to lead to its catalytic deficiency in phenol oxidation. It had been reported that iron oxide clusters exhibit an inactive catalytic performance in phenol degradation, due to its increased H_2O_2 decomposition which may be accompanied by iron leaching [43]. Thus, we believe that all these factors may have an influence in the poor catalytic performance of RH-15Fe and RH-20Fe compared to RH-10Fe.

3.2.6. The decomposition of H_2O_2 and catalytic reactivity

On the basis of stoichiometry in the oxidation of phenol, the molar ratio of H_2O_2 to phenol is 1:1. However our results indicated that a two-fold increase in H_2O_2 amount was required for an optimum conversion. This is due to the self-decomposition of H_2O_2 which is inevitable in the presence of highly active catalysts. Thus, we carried out the self-decomposition of H_2O_2 at different reaction temperatures as shown in Fig. 8.

In Fig. 8(a), it can be seen that the self-decomposition of H_2O_2 was very slow at both the temperatures studied, i.e. 303 and 343 K. At 303 K, the decomposition of H_2O_2 in the presence of the catalyst was almost the same as without the catalyst. However, at 343 K, the self-decomposition without the catalyst was slightly faster compared to 303 K. Even with the presence of the catalyst, the decomposition took 60 min for completion.

We also studied the decomposition of H_2O_2 in the presence of the reactant (phenol) and 30 mg catalyst (RH-10Fe) at 303 and 343 K with the same amount of oxidant. This is represented in Fig. 8(b). The decomposition of H_2O_2 occurred very fast in the presence of RH-10Fe and phenol. At 303 K, the decomposition was complete in 20 min. At 343 K however, it took less than 10 min for complete decomposition.

The decomposition of H_2O_2 can be represented by the following equations:

$$2H_2O_2 \underset{\text{Slow}}{\overset{\text{RH-10Fe}}{\rightleftharpoons}} O_2 + 2H_2O \quad (1)$$

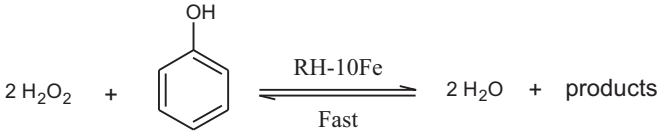

(2)

If free radicals are formed, then Eq. (1) will be fast and the attack on the phenol will be much more random. This will yield more than the observed number of products. As it is, Eq. (1) is slow and only in the presence of phenol, the reaction becomes fast as shown in Eq. (2). This means that the active intermediate and the phenol must come close to each other on the catalyst surface to cause reaction to occur. Also due to the structural morphology of the catalyst, only two products are observed.

This also explains the absence of an induction period in which the reaction proceeds very fast in this catalytic system.

3.3. Leaching and reusability of the catalyst

Table 4 presents the data obtained for the leaching test for RH-10Fe. The catalyst was removed after 2 min and the reagents were allowed to continue the reaction. A slight increase in phenol conversion was observed after the removal of catalyst, from 46.1 (2 min) to 50.3% (1 h). This could be due to the concentration effect arising from evaporation during the transfer of the reagents. However, at 2 h no increase in conversion (50.1%) was observed. Therefore, leaching of iron during phenol oxidation can be considered as insignificant. This implies that if there was Fe^{3+} that leached out of the catalyst, then there should have been a sig-

Table 4
Leaching test for RH-10Fe during the oxidation of phenol by H_2O_2.

Time (min)	Conversion (%)	Catechol (%)	Hydroquinone (%)
2	46.1	70.4	29.6
10[a]	47.4	67.5	32.5
20[a]	47.7	67.2	32.8
30[a]	48.8	63.0	37.0
60[a]	50.3	63.3	36.7
120[a]	50.1	63.6	36.4

Reaction conditions: phenol:H_2O_2 (molar ratio) 1:2; catalyst = RH-10Fe; the mass of catalyst used = 30 mg; T = 343 K; solvent = water (10 mL); time = 2 h.
[a] After removing the catalyst.

Table 5
Reusability of RH-10Fe under optimized reaction conditions.

Catalytic run	Phenol conversion (%)
1	95.2
2	91.1
3	85.5
4	82.1
5	79.3

nificant increase in the conversion of phenol. However, this was not observed. To further confirm the heterogeneity of the iron silica system, RH-10Fe catalyst after leaching test was subjected for AAS. It was found that iron content after leaching test was 7.38% as shown in Table 1. Insignificant reduction in iron content during the reaction confirms RH-10Fe is not prone to much leaching. It can thus be concluded that the catalytic oxidation of phenol by RH-10Fe proceeds via heterogeneous.

Although the colour of the reaction mixture was slightly dark, formation of tar can be considered negligible under the reaction conditions due to similar CAT/HQ ratio obtained when the reaction was proceeded to 6 h reaction time – (CAT/HQ = 1.57 (at 10 min), 1.58 (at 120 min), 1.55 (at 180 min) and 1.60 (at 360 min). This assumption was further confirmed when the catalyst was successfully regenerated by a simple physical process which will be made impossible if tar was present.

The reusability of RH-10Fe was carried out over several consecutive runs. It was observed that after five runs, the catalyst suffered a 16% drop in the catalytic activity (Table 5). The iron content after 4th reused was subjected for AAS analysis as shown in Table 1. These results conclude that the catalyst can be regenerated without any major loss in phenol conversion. However, the method of regeneration needs to be optimized further to improve catalytic efficiency.

Ahn and co-workers [22] reported a conversion of only 13% for Fe-MCM-41 at 50 °C on the third catalytic run with 30 mg of the catalyst and phenol:H_2O_2 ratio of 1:1 and 15 mL of water as solvent. It can thus be concluded that RH-10Fe is a better catalyst than Fe-MCM-41 or other catalyst reported in the literature.

3.4. The proposed mechanism of the catalytic reaction

Several authors have attributed the oxidation of phenol by H_2O_2 to a free radical mechanism [22,24,59]. It is normal that in a free radical mechanism the formation of benzoquinones were observed leading further to the formation of polymeric materials and tar formation. However, in this work benzoquinones were not observed. Due to this observation, a non-free radical mechanism is proposed for the conversion of phenol over RH-10Fe under the conditions studied. A similar mechanism was suggested by Mal et al. [60] for TS-1. According to ^{29}Si MAS NMR in Fig. 4, RH-10Fe has two possible silica structures which are Q^3 and Q^4 as depicted in Scheme 1. We believe that the intermediate will form on the catalyst sur-

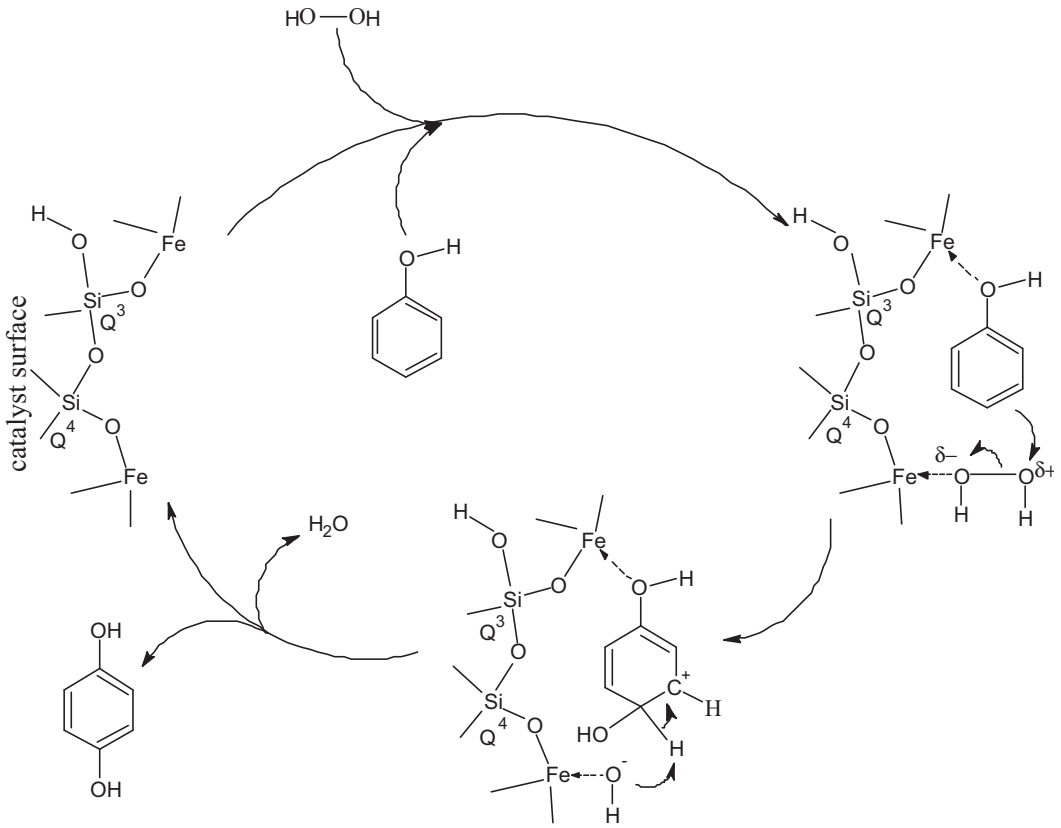

Scheme 1. The catalytic cycle for the oxidation of phenol by H_2O_2 in the presence of RH-10Fe. The mechanism shows the formation of hydroquinone. A similar mechanism may also be envisaged for the formation of catechol.

face assisted by the formation of coordinate bonds by the reactants to the Fe^{3+} active centers. We propose both reactants (phenol and H_2O_2) were adsorbed on the catalyst surface via hydrogen bonding.

4. Conclusions

This study shows the remarkable activity of high surface area and mesoporous iron incorporated rice husk silica catalysts for the oxidation of a hazardous pollutant, phenol. The enhanced textural properties and well dispersed iron species achieved in RH-10Fe greatly influences its high activity towards phenol conversion. Leaching of metal species was found to be insignificant. The prepared catalysts were found to be stable and could be reused several times.

Acknowledgment

We thankfully acknowledge the Malaysia Government for the E-Science Fund grant (No. 305/PKIMIA/613317) which had partly supported this work.

References

[1] A. Santos, P. Yustos, S. Rodriguez, F. Garcia-Ochoa, Wet oxidation of phenol, cresols and nitrophenols catalyzed by activated carbon in acid and basic media, Appl. Catal. B 65 (2006) 269–281.
[2] S. Ray, S.F. Mapolie, J. Darkwa, Catalytic hydroxylation of phenol using immobilized late transition metal salicylaldimine complexes, J. Mol. Catal. A: Chem. 267 (2007) 143–148.
[3] V. Rives, O. Prieto, A. Dubey, S. Kannan, Synergistic effect in the hydroxylation of phenol over CoNiAl ternary hydrotalcites, J. Catal. 220 (2003) 161–171.
[4] S. Kannan, A. Dubey, H. Knozinger, Synthesis and characterization of CuMgAl ternary hydrotalcites as catalysts for the hydroxylation of phenol, J. Catal. 231 (2005) 381–392.
[5] C. Samanta, Direct synthesis of hydrogen peroxide from hydrogen and oxygen: an overview of recent developements in the process, Appl. Catal. A 350 (2008) 133–149.
[6] F.P. Ballistreri, G.A. Tomaselli, R.M. Toscano, Selective and mild oxidation of thiols to sulfonic acids by hydrogen peroxide catalyzed by methyltrioxorhenium, Tetrahedron Lett. 49 (2008) 3291–3293.
[7] S. Shylesh, T. Radhika, K.S. Rani, S. Sugunan, Synthesis, characterization and catalytic activity of Nd_2O_3 supported V_2O_5 catalysts, J. Mol. Catal. A: Chem. 236 (2005) 253–259.
[8] J. Yu, P. Yang, Y. Yang, T. Wu, J.R. Parquette, Hydroxylation of phenol with hydrogen peroxide over tungstovanadophosphates with Dawson structure, Catal. Commun. 7 (2006) 153–156.
[9] M. Luo, D. Bowden, P. Brimblecombe, Catalytic property of Fe–Al pillared clay for Fenton oxidation of phenol by H_2O_2, Appl. Catal. B 85 (2009) 201–206.
[10] M.R. Maurya, A.K. Chandrakar, S. Chand, Oxidation of phenol, styrene and methyl phenyl sulfide with H_2O_2 catalysed by dioxovanadium(V) and copper(II) complexes of 2-aminomethylbenzimidazole-based ligand encapsulated in zeolite-Y, J. Mol. Catal. A: Chem. 263 (2007) 227–237.
[11] M.R. Maurya, S.J.J. Titinchi, S. Chand, Catalytic activity of chromium(III), iron(II) and bismuth(III) complexes of 1,2-bis(2-hydroxybenzamido)ethane (H_2hybe) encapsulated in zeolite-Y for liquid phase hydroxylation of phenol, J. Mol. Catal. A: Chem. 214 (2004) 257–264.
[12] S.W. Brown, A. Hackett, A.M. King, A. Johnstone, W.R. Sanderson, Catalytic hydroxylation of phenol, US Patent 5364982, 1994.
[13] F.S. Xiao, J. Sun, X. Meng, R. Yu, H. Yuan, D. Jiang, S. Qiu, R. Yu, A novel catalyst of copper hydroxyphosphate with high activity in wet oxidation of aromatics, Appl. Catal. A 207 (2001) 267–271.
[14] A.E. Ahmed, F. Adam, Indium incorporated silica from rice husk and its catalytic activity, Microporous Mesoporous Mater. 103 (2007) 284–295.
[15] F. Adam, P. Retnam, A. Iqbal, The complete conversion of cyclohexane into cyclohexanol and cyclohexanone by a simple silica–chromium heterogeneous catalyst, Appl. Catal. A 357 (2009) 93–99.
[16] F. Adam, C.L. Fook, Chromium modified silica from rice husk as an oxidative catalyst, J. Porous Mater. 16 (2009) 291–298.
[17] F. Adam, A.E. Ahmed, L.M. Sia, Silver modified porous silica from rice husk and its catalytic potential, J. Porous Mater. 15 (2008) 434–444.
[18] T. Radhika, S. Sugunan, Influence of surface and acid properties of vanadia supported on ceria promoted with rice husk silica on cyclohexanol decomposition, Catal. Commun. 7 (2006) 528–533.
[19] F. Adam, K. Kandasamy, S. Balakrishnan, Iron incorporated heterogeneous catalyst from rice husk ash, J. Colloid Interface Sci. 304 (2006) 137–143.
[20] F. Adam, A.E. Ahmed, The benzylation of xylenes using heterogeneous catalysts from rice husk ash silica modified with gallium, indium and iron, Chem. Eng. J. 145 (2008) 328–334.
[21] F. Adam, J. Andas, Amino benzoic acid modified silica—an improved catalyst for the mono-substituted product in the benzylation of toluene with benzyl chloride, J. Colloid Interface Sci. 311 (2007) 135–143.
[22] J.-S. Choi, S.S. Yoon, S.H. Jang, W.S. Ahn, Phenol hydroxylation using Fe-MCM-41 cataysts, Catal. Today 111 (2006) 280–287.
[23] H. Liu, G. Lu, Y. Guo, Y. Guo, Synthesis of TS-1 using amorphous SiO_2 and its catalytic properties for hydroxylation of phenol in fixed-bed reactor, Appl. Catal. A (2005) 153–161.
[24] L. Wang, A. Kong, B. Chen, H. Ding, Y. Shan, M. He, Direct synthesis, characterization of Cu-SBA-15 and its high catalytic activity in hydroxylation of phenol by H_2O_2, J. Mol. Catal. A: Chem. 230 (2005) 143–150.
[25] C. Xiong, Q. Chen, W. Lu, H. Gao, W. Lu, Z. Gao, Novel Fe-based complex oxide catalysts for hydroxylation of phenol, Catal. Lett. 69 (2000) 231–236.
[26] J. Mendham, R.C. Denney, J.D. Barnes, M. Thomas, Vogel's Textbook of Quantitative Chemical Analysis, 6th ed., Prentice Hall, 2000, pp. 435-436.
[27] M.R. Maurya, S.J.J. Titinchi, S. Chand, Liquid-phase catalytic hydroxylation of phenol using Cu(II), Ni(II) and Zn(II) complexes of amidate ligand encapsulated in Zeolite-Y as catalysts, Catal. Lett. 89 (2003) 219–227.
[28] R. Akkari, A. Ghorbel, N. Essayem, F. Figueras, Sulfated zirconia grafted on a mesoporous silica aerogel: influence of the preparation parameters on textural, structural and catalytic properties, Microporous Mesoporous Mater. 111 (2008) 62–71.
[29] J Li, X. Xu, Z. Hao, W. Zhao, Mesoporous silica supported cobalt oxide catalysts for catalytic removal of benzene, J. Porous Mater. 15 (2008) 163–169.
[30] D.-G. Choi, S.-M. Yang, Effect of two-step sol–gel reaction on the mesoporous silica structure, J. Colloid Interface Sci. 261 (2003) 127–132.
[31] P. Fabriozioli, T. Bürgi, M. Burgener, S. van Doorslaer, A. Baiker, Synthesis, structural and chemical properties of iron oxide silica aerogels, J. Mater. Chem. 12 (2002) 619–630.
[32] Q. Wu, X. Hu, P.L. Yue, X.S. Zhao, G.Q. Lu, Copper/MCM-41 as catalyst for the wet oxidation of phenol, Appl. Catal. B 32 (2001) 151–156.
[33] R.L. McCormick, G.O. Alptekin, D.L. Williamson, T.R. Onho, Methane partial oxidation by silica-supported iron phosphate catalyst. Influence of iron phosphate content on selectivity and catalyst surface, Top Catal. 10 (2000) 115–122.
[34] Y. Liu, K. Murata, M. Inaba, Direct oxidation of benzene to phenol by molecular oxygen over catalytic systems containing $Pd(OAc)_2$ and heteropolyacid immobilized on HMS or PIM, J. Mol. Catal. A: Chem. 256 (2006) 247–255.
[35] S. Ponce-Castañeda, J.R. Martínez, F. Ruiz, S. Palomares-Sánchez, O. Domínguez, Synthesis of Fe_2O_3 species embedded in a silica xerogel matrix: a comparative study, J. Sol–Gel Sci. Technol. 25 (2002) 29–36.
[36] M. Selvaraj, P.K. Sinha, K. Lee, I. Ahn, A. Pandurangan, T.G. Lee, Synthesis and characterization of Mn-MCM-41 and Zr–Mn-MCM-41, Microporous Mesoporous Mater. 78 (2005) 139–149.
[37] M.A. Figueiredo, A.L. de Faria, M. das Dores Assis, H.P. Oliveira, Synthesis by sol–gel process, characterization and catalytic activity of vanadia–silica mixed oxides, J. Non-Cryst. Solids 351 (2005) 3624–3629.
[38] Y. Yu, G. Xiong, C. Li, F.-S. Xiao, Characterization of iron atoms in the framework of MFI-type zeolites by UV resonance Raman spectroscopy, J. Catal. 194 (2000) 487–490.
[39] C. Li, Identifying the isolated transition metal ions/oxides in molecular sieves and on oxide supports by UV resonance Raman spectroscopy, J. Catal. 216 (2003) 203–212.
[40] Y. Li, Z. Feng, Y. Lian, K. Sun, L. Zhang, G. Jia, Q. Yang, C. Li, Direct synthesis of highly ordered Fe-SBA-15 microporous materials under weak acidic conditions, Microporous Mesoporous Mater. 84 (2005) 41–49.
[41] H. Xin, J. Liu, F. Fan, Z. Feng, G. Jia, Q. Yang, C. Li, Mesoporous ferrosilicates with high content of isolated iron species synthesized in mild buffer solution and their catalytic application, Microporous Mesoporous Mater. 113 (2008) 231–239.
[42] P. Nagaraju, Ch. Shrilakshmi, N. Pasha, N. Lingaiah, I. Suryanarayana, P.S. Sai Prasad, Effect of method of preparation on the activity and selectivity of iron phosphate in the ammoxidation of 2-methyl pyrazine, Catal. Today 131 (2008) 393–401.
[43] M.N. Timofeeva, M.S. Mel'gunov, O.A. Kholdeeva, M.E. Malyshev, A.N. Shmakov, V.B. Fenelonov, Full phenol peroxide oxidation over Fe-MMM-2 catalysts with enhanced hydrothermal stability, Appl. Catal. B 75 (2007) 290–297.
[44] J. Pérez-Ramirez, J.C. Groen, A. Brückner, M.S. Kumar, U. Bentrup, M.N. Debbagh, L.A. Villaescusa, Evolution of isomorphously substituted iron zeolites during activation: comparison of Fe-beta and Fe-ZSM-5, J. Catal. 232 (2005) 318–334.
[45] J. Pérez-Ramirez, F. Kapteijn, A. Brückner, Active site structure sensitivity in N_2O conversion over FeMFI zeolites, J. Catal. 218 (2003) 234–238.
[46] Y. Sun, S. Walspurger, J. Philippe Tessonnier, B. Louis, J. Sommer, Highly dispersed iron oxide nanoclusters supported on ordered mesoporous SBA-15: a very active catalyst for Friedel-Crafts alkylations, Appl. Catal. A 300 (2006) 1–7.
[47] S.K. Badamali, P. Selvam, M. Murugesan, H. Kuwano, Spectroscopic investigation of Fe(III) in Fe-MCM-41, Bull. Catal. Soc. India 5 (2006) 150–154.
[48] S.K. Badamali, P. Selvam, Probing the Fe(III) sites in mesoporous FeMCM-41, Catal. Today 141 (2009) 103–108.
[49] S.B. Hong, C.G. Kim, Y.S. Uh, Y.K. Park, S.I. Woo, Preparation and characterization of Vanado-, Ferri-, and Gallosilicate catalysts in the presence of fluoride ions, Korean J. Chem. Eng. 9 (1992) 16–22.
[50] V. Umamaheswari, W. Bohlmann, A. Poppl, A. Vinu, M. Hartmann, Spectroscopic characterization of iron-containing MCM-58, Microporous Mesoporous Mater. 89 (2006) 47–57.

[51] F. Testa, F. Grea, G.D. Diodati, L. Pasqua, R. Aiello, G. Terwagne, P. Lentz, J.B. Nagy, Synthesis and characterization of Fe- and [Fe,Al]-MCM-22 zeolites, Microporous Mesoporous Mater. 30 (1999) 187–197.
[52] W. Zhao, Y. Luo, P. Deng, Q. Li, Synthesis of Fe-MCM-48 and its catalytic performance in phenol hydroxylation, Catal. Lett. 73 (2001) 2–4.
[53] H. Kosslick, G. Lischke, H. Landmesser, B. Parlitz, W. Storek, R. Fricke, Acidity and catalytic behaviour of substituted MCM-48, J. Catal. 176 (1998) 102–114.
[54] K.C. Gupta, A.K. Sutar, Catalytic activity of polymer anchored *N*,*N*′-bis(*o*-hydroxy acetophenone) ethylene diamine Schiff base complexes of Fe(III), Cu(II) and Zn(II) ions in oxidation of phenol, React. Funct. Polym. 68 (2008) 12–26.
[55] H. Suja, S. Sugunan, Iron promoted sulphated zirconia systems as efficient catalysts for phenol hydroxylation, Bull. Catal. Soc. India 2 (2003) 194–203.
[56] M. Constantini, E. Garcin, M. Gubelmann, J.M. Popa, Hydroxylation of phenols/phenol ethers, US Patent 5149888, 1992.
[57] N.K. Mal, A.V. Ramaswamy, Hydroxylation of phenol over Sn-silicalite-1 molecular sieve: solvent effects, J. Mol. Catal. A: Chem. 105 (1996) 149–158.
[58] A.F.J. Santiago, J.F. Sousa, R.C. Guedes, C.E.M. Jerônimo, M. Benachour, Kinetic and wet oxidation of phenol catalyzed by non-promoted and potassium-promoted manganese/cerium oxide, J. Hazard. Mater. B 138 (2006) 325–330.
[59] C. Liu, Y. Shan, X. Yang, X. Ye, Y. Wu, Iron(II)-8-quinolinol/MCM-41-catalyzed phenol hydroxylation and reaction mechanism, J. Catal. 168 (1997) 35–41.
[60] N.K. Mal, P. Kumar, M. Sasidharan, M. Matsukata, Modified TS-1 for shape selective phenol hydroxylation to hydroquinone, Stud. Surf. Sci. Catal. 154 (2004) 2618–2625.